

## Fabrication and characterization of polysulfone ultrafiltration membrane using polyethylene glycol and tartaric acid: morphology and performance in protein separation

N. Sharma\* and M.K. Purkait

Department of Chemical Engineering, Indian Institute of Technology Guwahati,  
Guwahati - 781039, Assam, India

(Received January 4, 2017, Revised July 3, 2017, Accepted August 15, 2017)

**Abstract.** Increase in the hydrophilicity (HPCT) of polysulfone (PS) membrane and subsequently decrease in fouling can be achieved by surface modification of PS based membranes. Therefore, in this work, ultrafiltration membranes with increased HPCT were prepared using the enantiomeric tartaric acid (D-TA) and racemic tartaric acid (DL-TA). Phase inversion technique was used for the preparation of polyethylene glycol and TA blended PS membrane. Morphological analysis of the fabricated membranes was done by scanning electron microscope and atomic force microscopy. Bovine serum albumin (BSA) solution was taken for finding the permeation and rejection behavior of prepared membranes. Maximum BSA rejection was increased by 70.5% for the modified membrane.

**Keywords:** polysulfone; tartaric acid; hydrophilicity; chirality; polyethylene glycol

---

### 1. Introduction

Polysulfone (PS) based asymmetric ultrafiltration (UF) membranes are widely used in water treatment, food processing and biotechnology (Cheryan 1998, Mulder 1996). This is one of the most promising clean energy technologies. PS have certain potential advantages, including its excellent acidic and basic resistance, good thermal stability, wide pH range and film forming ability (Bhadra *et al.* 2008, Geise *et al.* 2010, Kim *et al.* 1998, Tweddle *et al.* 1983). Major disadvantages of PS membranes include their low infiltration capacity and severe membrane fouling because of their hydrophobic nature (Zhang *et al.* 2008). It is very necessary to overcome these problems for increasing the permeability and life span of the membrane. Membrane fouling can be classified in two types; these are as reversible and irreversible fouling. Reversible adsorption and deposition of protein causes reversible fouling. This type of fouling can be removed by simple hydraulic cleaning. But irreversible protein adsorption causes irreversible fouling that can only be eliminated by chemical cleaning or enzymatic degradation (Kimmerle *et al.* 1990). Surface characteristics of membrane such as morphology, porosity, pore size and hydrophilicity (HPCT) affect the membrane fouling (Vatanpour *et al.* 2012). Flux-declining and

---

\*Corresponding author, Ph.D., E-mail: [s.nilay@iitg.ernet.in](mailto:s.nilay@iitg.ernet.in)

membrane fouling can be reduced by improving the HPCT of the membrane. Many researchers have done work by altering the composition of the membrane for finding an additional hydrophilic material. So, membrane fouling can be remarkably reduced by increasing the HPCT of the membrane surface as well as porous surfaces (Ahmad *et al.* 2013, Li *et al.* 2006). Surface modification of PS membrane can be done by blending of organic acids that result in increased hydrophilicity of the membrane.

BSA can bind a broad range of substances such as hormones, fatty acids, amino acids and a large variety of drugs. Consequently formed complexes that are involved in transport and regulatory processes and thus, they are enormously useful in biological processes (Sevilla *et al.* 2007). Serum protein adsorption onto PS membrane in different blood-contact applications can be the reason of life threatening complications (Wang *et al.* 2008). Hence, BSA was used for the characterization of membranes in this study. Sinha *et al.* (2015) synthesized polyurethane macromolecules (PU) with end capping of different organic acids. Membranes blended with PU showed improved pore density, HPCT and pure water flux compared to plain PS membrane. They observed that BSA flux recovery ratio was enhanced by the addition of PU for all the modified membranes. Sharma *et al.* (2016) studied the Racemic and enantiomeric effect of tartaric acid on the hydrophilicity of polysulfone membrane. They resulted with improved HPCT of synthesized membranes.

Ghaemi *et al.* (2012a) studied the xenobiotics removal at different solution pHs. Effect of several concentrations of different organic acids on the morphology and performance of PS membrane was investigated by them. They resulted with the fact that porosity was maximum for 0.5 wt % of all the organic acids in the PS membrane. They also observed the fact that increased zeta potential of the membrane caused increased xenobiotics rejection. Ghaemi *et al.* (2012b) also studied the effect of amphiphilic fatty acids (palmitic, oleic, and linoleic acid) on the structure and performance of cellulose acetate nano filtration membranes. They observed that addition of palmitic acid depicts higher rejection of nitrophenols than other fatty acids. Mansourizadeh *et al.* (2010) used Polyethylene glycol (PEG 200) and ethanol, glycerol and acetic acid as the additives in porous PS hollow fiber membranes for CO<sub>2</sub> absorption. They found that all the additives resulted in enhanced surface porosity. Wei *et al.* (2012) studied the effect of preadsorption of citric acid on surface modification of PS ultrafiltration membrane. They observed that after modification, the membrane surfaces became more hydrophilic and permeability also improved. The modified membranes showed enhanced BSA and PEG retentions and improved antifouling properties with higher flux recovery ratios. Acrylic acid was also used with different hydrophilic polymers (Li1 *et al.* 2013) for improving the antifouling properties of protein. Ingole *et al.* (2016) prepared the activated carbon incorporated polysulfone membranes for dye separation. Their study resulted with improved dye separation by the addition of activated carbon.

It appears from the recent literature that improved HPCT of polymeric membrane can be achieved by the addition of an organic acid. It is also found that although a lot of works have reported on the addition of different organic acids to polymeric membrane, but only few researchers have done work on enantiomeric and racemic effect of organic acids on membranes (Yang *et al.* 2009). In addition, D-TA and DL-TA possess different solubility in water as well as have different acid dissociation constants which can affect the porosity and surface charge of membrane. Therefore, in the present work a detailed study was done for finding the effects of addition of different amounts of D-TA and DL-TA (0.5 and 1 wt %) into the casting solution of PS membrane; in order to increase the HPCT and BSA rejection performance of PS membrane. PEG (400 Da) was taken as pore former in this study and blended in PS membrane casting solution.

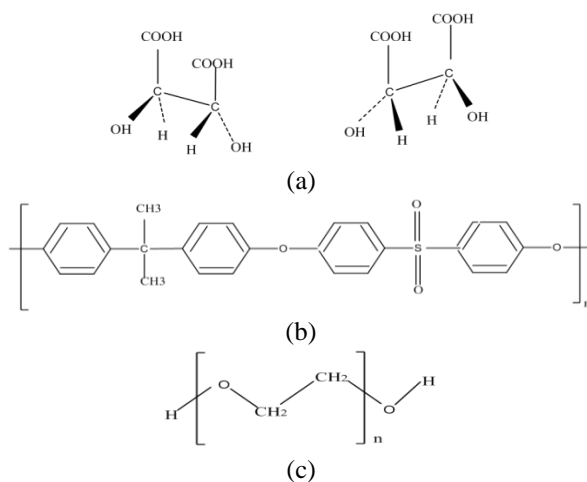


Fig. 1 (a) Chemical structure of D-Tartaric acid and L-Tartaric acid (b) Polysulfone (c) Polyethylene glycol (PEG)

Effects of chirality of TA on the HPCT, water flux as well as permeation and rejection behaviour of BSA under various solution conditions was studied. For characterizing the prepared membranes, morphological parameters were examined. FTIR-ATR, contact angle and zeta potential measurements were also performed. All the parameters were examined and explained well.

## 2. Experimental

### 2.1 Reagents and materials

Polysulfone (average molecular weight 30,000 Da) was procured by Sigma-Aldrich Co. USA and dimethyl acetamide (DMAc) supplied by LOBA Chemie, India were used as base polymer and solvent, respectively for membrane preparation. Sisco Research Laboratories Pvt. Ltd, Mumbai India, supplied the PEG (average molecular weight 400 Da), which was used as pore forming additive. D-tartaric acid ( $pK_a=2.98$ ) and DL-tartaric acid ( $pK_a=3.03$ ) with average molecular weight of 150 Da for both TAs and bovine serum albumin (molecular weight 68000 Da) were supplied by Otto Chemie Private Limited India. Chemical structures of PEG, D-tartaric acid, L-tartaric acid and PS are shown in Fig. 1.

### 2.2 Membrane fabrication

Flat sheet PS membrane fabrication was done by the wet phase inversion method using PEG (400 Da) with D-TA and DL-TA. The PS concentration was fixed at 18 wt % for all the membranes. PEG (2 wt %), D-TA and DL-TA (0.5 and 1 wt %) were used as additives (Table 1). Membranes with different compositions were designated as M-1, M-2, M-3, M-4 and M-5, containing different ratio of organic acids (i.e., D-TA and DL-TA) and solvent (i.e., DMAc). Magnetic stirrer was used for preparing the membrane casting solution. Detailed membrane

Table 1 Composition of PS casting solutions of the membranes

Serial No.	Membrane	PS (wt%)	PEG (wt%)	DMAc (wt%)	D-TA (wt%)	DL-TA (wt%)
M-1	Plain	18	2	80	-	-
M-2	D <sub>1</sub> PEG	18	2	79	1	-
M-3	D <sub>0.5</sub> PEG	18	-	79.5	0.5	-
M-4	DL <sub>1</sub> PEG	18	2	79	-	1
M-5	DL <sub>0.5</sub> PEG	18	-	79.5	-	0.5

fabrication procedure is discussed in our previous work (Sharma *et al.* 2015). Membranes thickness was maintained as 100  $\mu\text{m}$  for all the five membranes.

### 2.3 Characterization of membranes

Permeation experiments and morphological analysis were performed for the characterization of prepared membranes. Membrane performance was evaluated in terms of compaction factor (CF), equilibrium water content (EWC), pure water flux (PWF), BSA rejection percentage (% R). HPCT of membrane was measured by water contact angle. Zeta potential of membranes was measured by Delsa nano, Beckman coulter, Switzerland. The pore size distribution and porosity of the membrane are main factors for deciding its performance (Kamusewitz *et al.* 1997). Liquid-liquid displacement porosimetry (LLDP) method was used for the morphological analysis of the prepared membrane.

#### 2.3.1 Liquid-liquid displacement (LLDP) porosimetry method

Number of pores, mean pore size and cumulative permeability (%) with respect to pore size of the prepared membranes were determined by LLDP method (Mulder 1996). In this method, a suitable penetrating liquid was used for complete wetting of the membrane and then a liquid that can not wet the membrane was taken for pressurizing, to pass through the pores by displacing the liquid which was already filled in the pores (wetting liquid). The radius ( $r$ ) was calculated by renowned Cantor's equation

$$r = \frac{2\sigma}{P} \quad (1)$$

Where,  $P$  is the transmembrane pressure and  $\sigma$  is the interfacial tension between the two liquids. The total hydraulic permeability coefficient ( $L_n$ ) was calculated by

$$L_n = \sum L_{i,k} = \sum \frac{J_{i,k}}{P_{i,k}} \quad (2)$$

where  $J_{i,k}$  is flux at pressure  $P_{i,k}$  and  $L_{i,k}$  is partial permeability coefficient of the pores with radius  $r_i$  and  $r_k$  evaluated at  $P_{i,k}$ , which corresponds to a mean radius  $r_{i,k}$ .

$$r_{i,k} = \frac{r_i + r_k}{2} \quad (3)$$

Pore radius versus pore number and pore radius versus pore area curves can be obtained using

the following equations (Abaticchio *et al.* 1990)

$$N_{i,k} = \frac{d\eta}{2\pi\sigma^4} P^3 J_{i,k} \quad (4)$$

$$A_{i,k} = \pi r_{i,k}^2 N_{i,k} \quad (5)$$

where  $N_{i,k}$  is the pore density, i.e., the number of pores having radius between  $r_i$  and  $r_k$  per unit area of the membrane surface,  $d$  is the pore length which is nearly equal to width of the top skin layer and  $\eta$  is the viscosity of the alcohol rich mixture.  $A_{i,k}$  is the area of the pores having radii between  $r_i$  and  $r_k$ . Last two equations are found from the well known Hagen-Poiseuille's permeation equations with the assumption of cylindrical pores and laminar flow. Skin layer thickness was equal to 100 nm in this work. The total area  $A_t$  and total number of pores per unit area of the membrane  $N_t$  was calculated as follows

$$A_t = \sum A_{i,k} \quad (6)$$

$$N_t = \sum N_{i,k} \quad (7)$$

The mean pore radius  $r_m$  was calculated as (Cappanelli *et al.* 1983)

$$r_k = \frac{\sum N_{i,k} r_{i,k}}{\sum N_{i,k}} \quad (8)$$

The inadequacy of this method is that the absolute values of  $A_t$ ,  $N_t$  and their distribution probably have an error due to the deviation from the hypothesis of cylindrical pores and inconsistent thickness of membranes skin layer (Sinha *et al.* 2013). Though, the results are possibly helpful for the comparison of various membranes.

### 2.3.2 Permeation experiments

Batch experiments were performed in a dead-end, stainless steel cell discussed in our previous work (Sharma *et al.* 2015). Nitrogen gas of normal purity was used for pressurizing the cell to an operating pressure of 208 kPa. Before the experiments membranes were compacted at 345 kPa. Permeate was collected from the lower side of the cell. Compaction factor (CF) was determined by standard technique (Chakrabarty *et al.* 2008).

### 2.3.3 Hydraulic permeability ( $P_m$ ) and pure water flux (PWF)

Deionized water was permitted to move across the compacted membrane for finding the pure water flux (PWF). Pure water flux at different trans membrane pressures (upto 345 kPa) was calculated using the following equation

$$J_w = \frac{Q}{A\Delta t} \quad (9)$$

where,  $J_w$  is the pure water flux ( $L/m^2 h$ ),  $Q$  is the volume of permeated water ( $L$ ),  $A$  is the effective membrane area ( $m^2$ ),  $t$  is the permeation time and slope of the  $J_w$  vs  $P$  plot gave the  $P_m$  ( $L/m^2 h kPa$ ) (Sinha *et al.* 2015).

### 2.3.4 HPCT and membrane resistance

Static contact angle was measured for finding the HPCT of membrane. Detailed information is given in our previous works (Sharma *et al.* 2015, Sinha *et al.* 2013). Membrane resistance was calculated by the following equation

$$R_m = \frac{P_T}{\mu J_{water}} \quad (10)$$

Where,  $J_{water}$  is PWF,  $P_T$  is the pressure,  $\mu$  is the viscosity of water and  $R_m$  is membrane resistance.

### 2.4 Ultrafiltration experiment

Stainless steel batch cell was used for performing ultrafiltration experiments, explained in literature (Sharma *et al.* 2015) to study the effects of chirality of tartaric acid on permeate flux as well as solute separation performance of the prepared membranes. Bovine Serum Albumin (BSA) protein was taken as solute for the permeation experiments. Concentration of BSA Solution was taken as 1000 mg L<sup>-1</sup> for all the permeation and separation experiments. The pH of BSA solution was taken approximately at five values: 3, 4.8, 7, 8 and 10. The BSA rejection ratio was measured by the following equation:

$$R\% = \left(1 - \frac{C_p}{C_f}\right) \times 100 \quad (11)$$

where,  $C_f$  concentrations in the feed and  $C_p$  concentrations in the permeate in mg/mL, respectively. Concentration of BSA was measured for 5h, the permeate sample was collected at every 1h period of ultrafiltration. UV-vis Spectro-photometer (Perkin-Elmer Precisel, Lamda-35) was used for finding the concentrations of BSA in permeate, at wavelength of 280 nm.

### 2.5 Fouling study

Membrane fouling causes flux loss ( $J_{w1}-J_p$ ). To study the antifouling property, Cheryan (1998) defined some ratios to describe the fouling process. The first ratio is  $F_t$ , which is the degree of total flux loss caused by total fouling.  $F_t$  was calculated by following equation

$$F_t = 1 - \frac{J_p}{J_{w1}} \quad (12)$$

$F_r$  and  $F_{ir}$  are other two ratios. Where,  $F_r$  is reversible fouling and  $F_{ir}$  is irreversible fouling.  $F_r$  and  $F_{ir}$  were calculated by the following equations

$$F_r = \frac{J_{w2} - J_p}{J_{w1}} \quad (13)$$

$$F_{ir} = \frac{J_{w1} - J_{w2}}{J_{w1}} \quad (14)$$

Where,  $J_{w1}$  is initial water flux (L/m<sup>2</sup>h) and  $J_{w2}$  is water flux in second run (L/m<sup>2</sup>h) and  $J_p$  is BSA solution flux (L/m<sup>2</sup>h). The reversible BSA adsorption on the membrane surface causes

reversible fouling, which can be eliminated by hydraulic cleaning. Irreversible fouling caused by irreversible BSA adsorption, cannot be avoided by hydraulic washing. Thus  $F_t$  is sum of  $F_r$  and  $F_{ir}$ .

$$F_t = F_r + F_{ir} \quad (15)$$

### 3. Results and discussion

#### 3.1 FTIR-ATR spectroscopy analysis of different membranes

For the confirmation of whether D-TA and DL-TA were retained or not in casted membrane matrix, FTIR-ATR spectra of plain M-1 membrane, D-TA and DL-TA containing M-2 and M-4 membranes was taken. Fig. 2 (a), (b) and (c) depict the spectra for membrane M-1, M-2 and M-4, respectively. Fig. 2(a) shows the peak at  $686 \text{ cm}^{-1}$  is the characteristic band of the plane aromatic C-H bond in PS membrane, stretching at  $851 \text{ cm}^{-1}$  represents S-O-C, symmetric and asymmetric stretching of sulfonate groups are presented by peaks  $1140 \text{ cm}^{-1}$  and  $1250 \text{ cm}^{-1}$ , respectively. The strong absorption peak at  $1500 \text{ cm}^{-1}$  is characteristic peak of C=C which is related to the stretching benzene ring skeletal. Peak found at  $3744 \text{ cm}^{-1}$  in FTIR-ATR spectra of PS based membrane is related to -OH groups of PEG molecules which added as the pore former to PS casting solution. A few groups were remained there in the membrane matrix because it was not completely washed away during wet phase inversion (Kobayashi *et al.* 2002, Liou *et al.* 2011, Silverstein *et al.* 1991).

Fig. 2 (b) and (c) represent the FTIR spectra of D-TA and DL-TA membranes with 1 wt %. Peak at  $3601 \text{ cm}^{-1}$  confirms the presence of small amount of TA in both the membranes after fabrication process (Stuart 2004).

#### 3.2 Morphological study

AFM images were used for finding the surface roughness parameters. Whereas, size and shape of the pores on the membrane surface were examined by high resolution field emission scanning electron microscope (FESEM). Cross-sectional morphology of the prepared membranes was analyzed by SEM images, since lower magnification was sufficient for finding the cross sectional morphology of the pores.

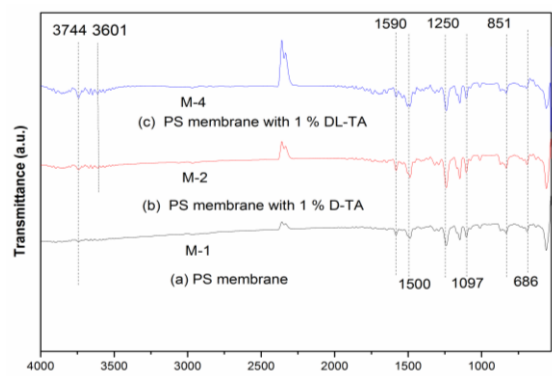


Fig. 2 FTIR-ATR spectra of M-1, M-2 and M-4 membranes

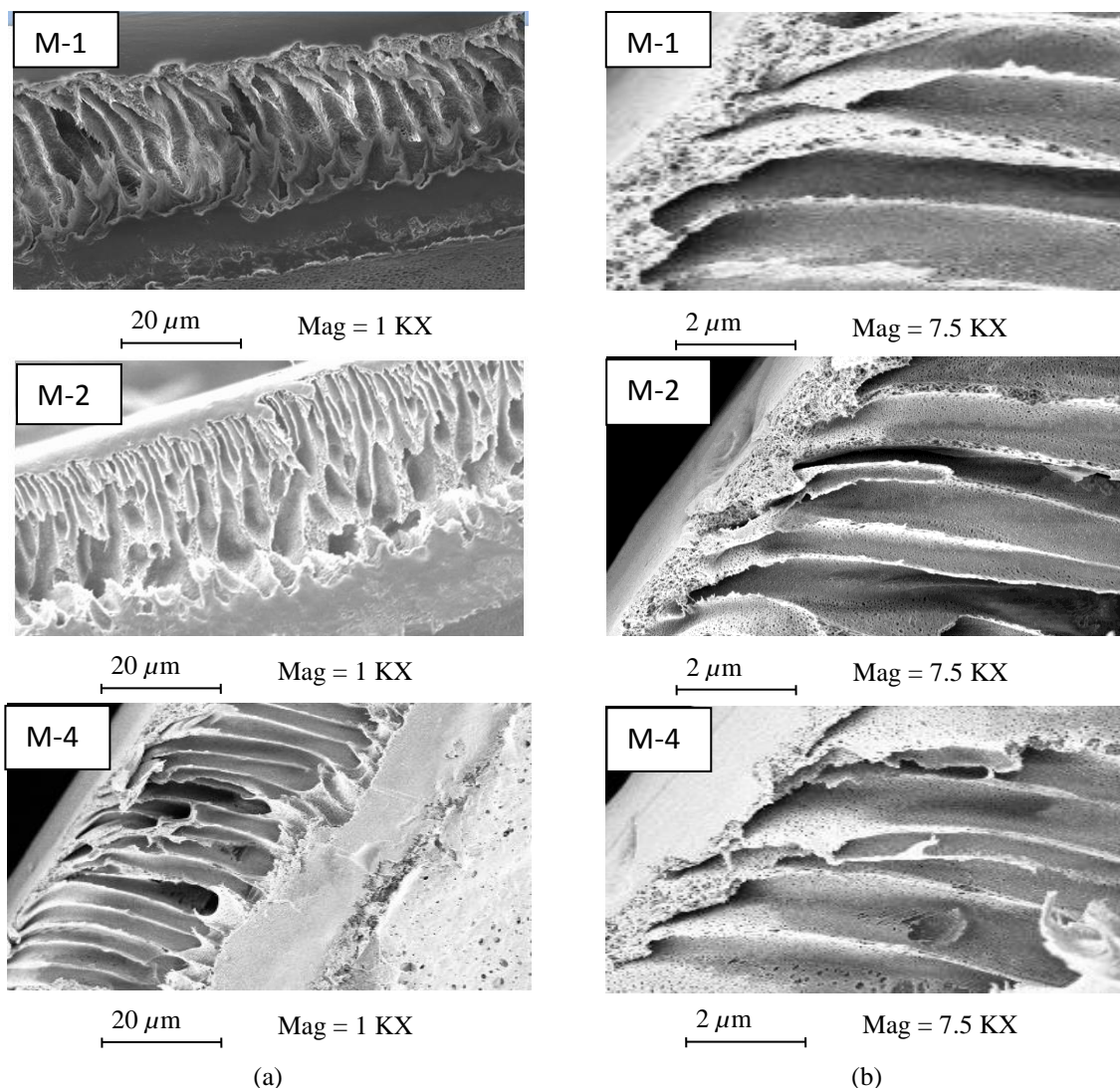


Fig. 3 SEM images of M-1, M-2 and M-4 at different magnifications

### 3.2.1 SEM image analysis

Fig. 3 depicts the SEM images of the cross-sectional view of M-1, M-2 and M-4 membranes (Table 1) with lower and higher magnification. Structure of both the membranes depicts a dense top layer and a permeable sub-layer, which was almost common for both the membranes. The thickness of top layer (active layer) changed by the addition of D-TA in the membranes. Finger-like structure was appeared on the porous sub-layer. Since, DMAc shows high interactive affinity with water; DMAc goes to water bath and simultaneously water comes to the membrane matrix, instantaneous demixing resulted in the groove like cavities in the sub-layer of the prepared membranes (Mulder 1996). This fact can also be explained by the information that addition of an additive into the casting solution causes kinetic hindrance against phase separation by increasing the viscosity of the solution. Throughout the process, non-solvent concentration in the polymer

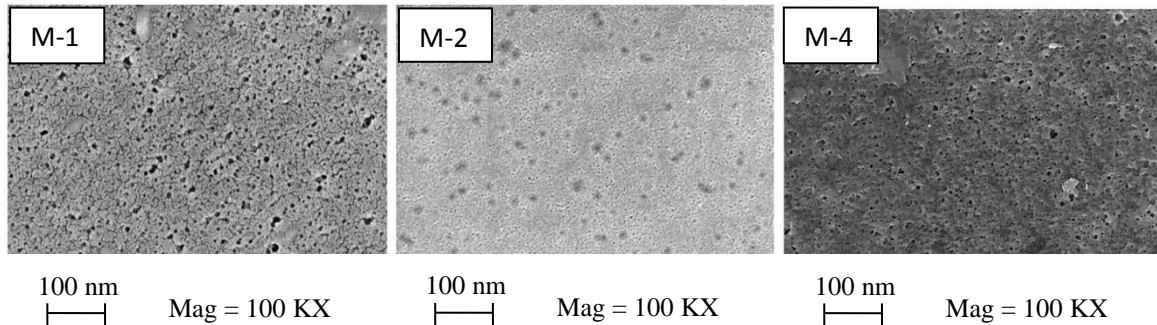


Fig. 4 Top surface FESEM images

solution rises until the demixing gap is achieved (Duarte *et al.* 2012). Structural analysis of the membranes can be done by the phase separation theory. Top layer thickness of both the membranes M-2 and M-4 got reduced and porosity increased as compared to plain membrane M-1, possibly due to the interactions between ingredients in the casting solution Ghaemi *et al.* (2012a). Tartaric acid present in the casting solution forms hydrogen bonds between oxygen atoms of polymer chains and hydrogen atoms of tartaric acid. Consequently bonds became weak between polymers chain; and faster phase separation occurred in the case of M-2 and M-4 membranes.

### 3.2.2 FESEM analysis

Fig. 4 depicts the top surface images of M-1, M-2 and M-4 membranes captured by FESEM. Dense top layer on the membrane surface was developed by spinodal demixing. This may be because of the fact that the diffusion process between coagulation medium and polymer solution was so fast to become extremely unstable and cross the spinodal curve during formation of top layer (Kimmerle *et al.* 1990, Reuvers *et al.* 1987). Pore size analysis of images taken by FESEM was done by Image *J* software (Hand *et al.* 2009). Mean pore size was measured 12.43 nm, 9.41 nm and 10.69 nm for M-1, M-2 and M-4, respectively. It was confirmed that addition of D-TA and DL-TA reduced the pore size of the membrane with different concentration of D-TA and DL-TA in PEG (400 Da) containing membrane.

### 3.2.3 AFM analysis

Atomic force microscopy (AFM) was used for analyzing the surface morphology and roughness of the membranes. Small squares of membranes (Approximately  $1.5 \text{ cm}^2$ ) were taken for study. WSxM software was used for image analysis. Fig. 5 depicts the AFM images of all the 5 membranes. Average height ( $S_z$ ), root mean square (RMS) roughness ( $S_q$ ) and Average Roughness ( $S_a$ ) were measured. RMS roughness was found to be increased with the addition of both D-TA and DL-TA. Further it was also observed that D-TA containing membranes show more RMS roughness than DL-TA containing membranes (Table 2). It may be attributed to the fact that porosity was increasing since number of pores on the surface was increasing by the addition of D-TA as compared to DL-TA. Table 2 shows different surface roughness parameters. PS membrane M-1 has a surface with compacted structure as shown in Fig. 5(a), in contrast M-2, M-3, M-4 and M-5 membrane Fig. 5(b) has an uneven surface with lots of small pores, thus higher surface porosity. The contact angle also decreased with the addition of TA and was measured as  $79^\circ$ ,  $57^\circ$ ,  $61^\circ$ ,  $68^\circ$  and  $71^\circ$  for M-1, M-2, M-3, M-4 and M-5, respectively. Hydrophilic behavior of the

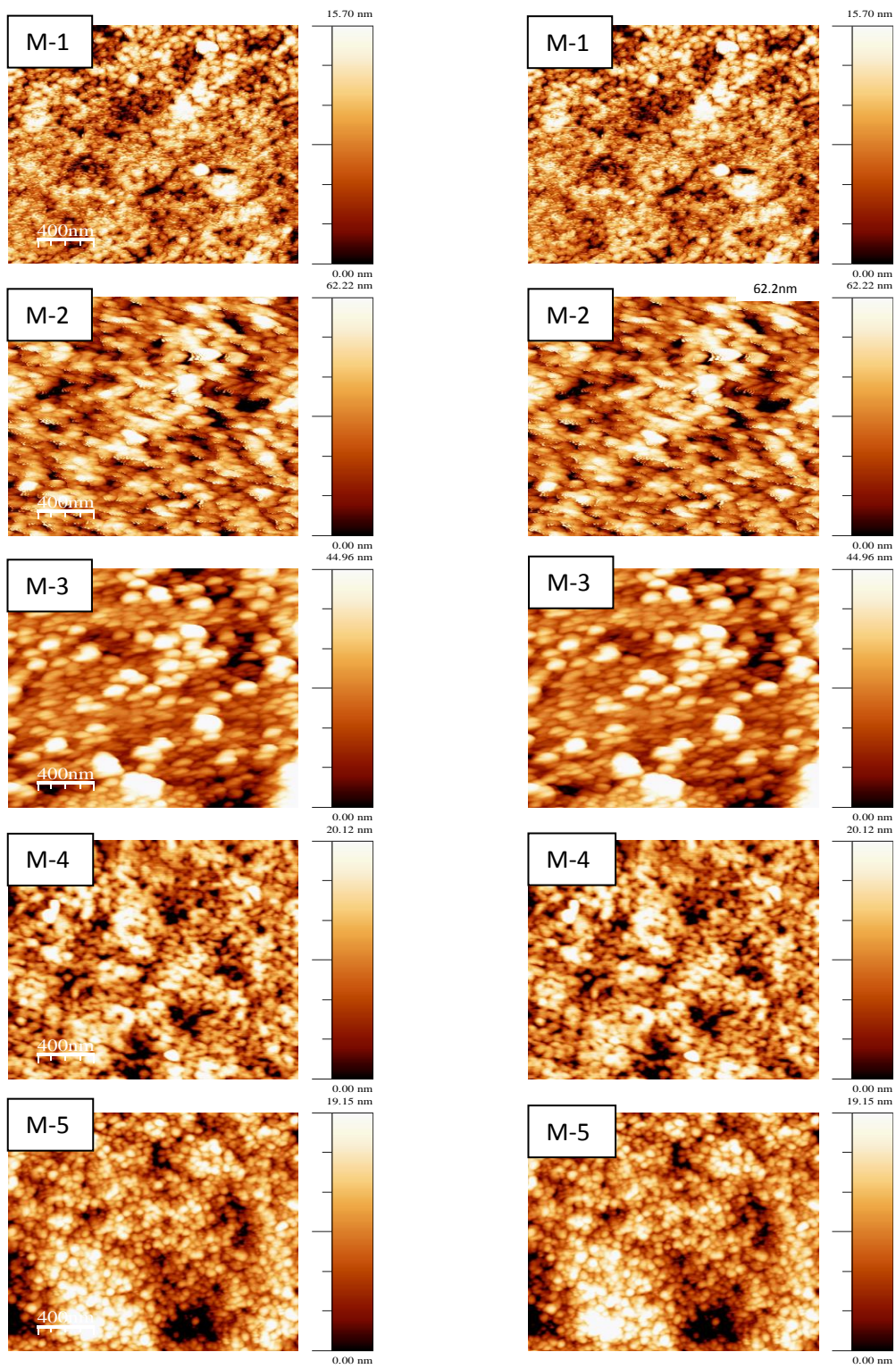


Fig. 5 2D and 3D AFM images of membranes

Table 2 Surface roughness and other characterization parameters of the membranes

Serial No.	Membrane	Roughness parameters			Pore number $N_p \times 10^{-8} (\text{m}^2)$	Zeta Potential (mV) at pH 7.5
		$S_z$ (nm)	$S_q$ (nm)	$S_a$ (nm)		
M-1	Plain	2.2	1.4	1.7	0.86	-8.11
M-2	D <sub>1</sub> PEG	15	5.8	6.7	2.5	-18.39
M-3	D <sub>0.5</sub> PEG	12.8	5.3	5.1	1.8	-17.16
M-4	DL <sub>1</sub> PEG	10.7	4.9	2.7	1.4	-17.58
M-5	DL <sub>0.5</sub> PEG	4.1	3.9	2.5	0.93	-16.75

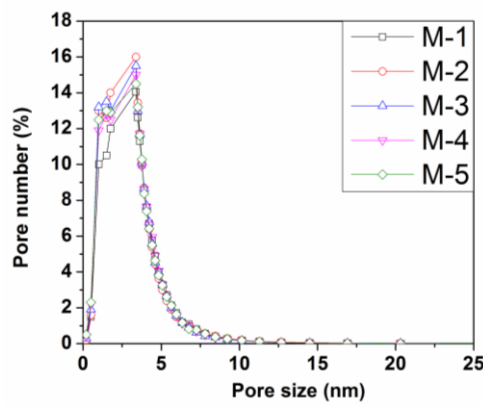


Fig. 6 Pore size distribution of all the membranes by LLDP method

membrane is explained by water contact angle measurement. Lower the WCA value higher will be the hydrophilicity of the membranes and more hydrophilic membranes are less prone towards fouling. Pore area and number of pores also increased by blending of both D-TA and DL-TA. It indicates increasing HPCT with addition of both TA's in this study. Between D-TA and DL-TA former gave better HPCT for example contact angle for M-2, and M-4 was  $57^\circ$  and  $68^\circ$ , respectively. It may be probably because of the fact of the more solubility of D-TA in water than DL-TA and molecules of L-TA also retained inside the membrane matrix as polarimeter did not show any enantiomer traces for the PWF collected from DL-TA containing membrane. Thus, more pores were formed by the addition of D-TA.

#### 3.2.4 Analysis of liquid-liquid displacement porosimetry results

Radius of the pore, permeability of the membranes, pore number per unit area and area of the pores for each membrane were calculated using Eqs. (1), (2), (4) and (5), respectively. Pore size distribution of the membranes observed by LLDP is shown in Fig. 6. Around 16% of the pores were in the size of 2-3 nm for M-2. For M-1, M-3, M-4 and M-5 these numbers are 14.1%, 15.5%, 15% and 14.4%, respectively. It can be seen from the figure 6 that the pores approximately 90% for all the five membranes are in the range of 3-5 nm which clearly brought them under UF range. Fig. 7 depicts the Variation in cumulative permeability (%) with pore size (nm). Though, larger pores play major role in overall permeability; as contribution from the small number of larger pores (>50 nm) can be quite high compared to the smaller size pores (<5 nm) though they are majority in number (Chakrabarty *et al.* 2008). Hagen-Poisuille equation explains that the enlarged

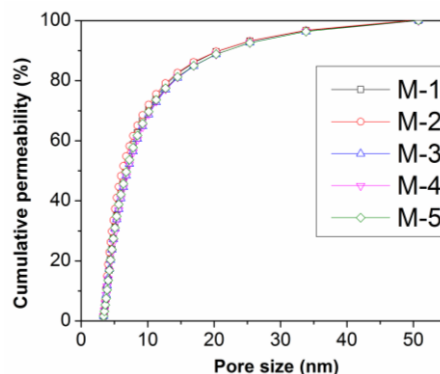


Fig. 7 Variation in cumulative permeability (%) with pore size (nm)

pore radius can be responsible for increase in flux. Calvo *et al.* (2004) observed the same results for UF membranes formed by track etched method. However, it is difficult and challenging to measure the accurate part of the larger pores (>50 nm) and smaller pores (<2 nm) by the LLDP method. Results obtained by LLDP method are placed in Table 2. It is observed that, by the addition of both D-TA and DL-TA number of pores for all the membranes increases; especially addition of D-TA resulted in more porous membranes. Pores were increased from  $0.86 \times 10^8 \text{ m}^{-2}$  to  $2.5 \times 10^8 \text{ m}^{-2}$  for membrane M-1 and M-2, respectively. The mean pore size  $r_m$  for all the five membranes was slightly decreased by the addition of TAs. It was calculated as 1.98 nm, 1.39 nm, 1.41 nm, 1.43 nm and 1.5 nm for M-1, M-2, M-3, M-4 and M-5, respectively.

### 3.3 Permeation studies

PS/PEG/TA/DMAc blended membranes were checked by permeation behavior. Characterization of the membranes was done in terms of CF, PWF and hydraulic permeability. Lastly, the membranes were examined for its permeation and rejection behavior with BSA protein at several pHs.

#### 3.3.1 Effect of chirality of TA on CF

Compaction factor (CF) has significance for describing the structure of the membrane. Increased CF shows that the membrane would be more compacted as sublayer owns more macrovoids. Membranes compaction was done at 345 kPa for 1 h. After that operating pressure was maintained at 208 kPa for next 1h during pure water flux collection. Fig. 8 shows the flux profile during compaction, it was observed that initial PWF was maximum for both the D-TA containing membranes whereas flux was least for the membrane without any TA. It may be because of the fact that addition of tartaric acid to the casting solution is the reason of unsteadiness in thermodynamic equilibrium of the system Ghaemi *et al.* (2012 a). Thus, increased demixing rate was responsible for highly porous membranes. However, membranes with D-TA gave higher flux than DL-TA membranes with constant molecular weight of PEG (400 Da). It may be because of the fact that DL-TA is less soluble than D-TA in coagulation medium (water).

#### 3.3.2 Effect of D-TA and DL-TA on compaction behavior, hydraulic permeability and PWF

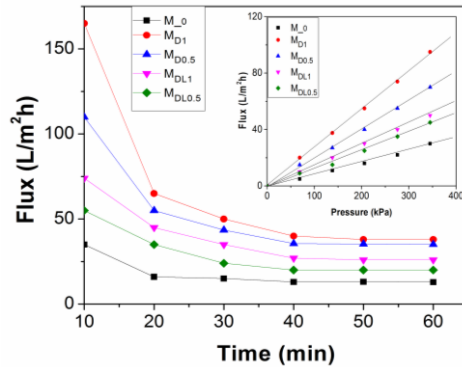


Fig. 8 Flux profile during compaction at 345 kPa and effect of transmembrane pressure on PWF

Left part of Fig. 8 shows effect of compaction time on PWF. PWF is initially found to be decreased sharply with time for all the membranes probably as a result of compaction and finally achieve a constant flow rate after around 0.5 h. This may be because of the pore size reduction. Since, the walls of the sublayer pores became narrower, denser and uniform (Qiu *et al.* 2009). It was observed from the figure that the steady state PWF increased when both the TAs were added. For example, the steady state flux increases from around 13.32 L/m<sup>2</sup>h to 38.01 L/m<sup>2</sup>h, when D-TA was added to the membrane and also increases from 13.32 L/m<sup>2</sup>h to 26.04 L/m<sup>2</sup>h by the addition of DL-TA to the membrane with PEG (400 Da). Table 3 presents the CF for the membranes. The main observation was that PS/DMAc/PEG/D-TA membranes acquire highest CF than both DL-TA containing membranes and without any acid containing membrane. The CF decreases from 4.3 to 2.7 for membrane M-1 and M-2, respectively. Since, addition of two additives and type of solvent used into the membrane casting solution can act as either enlarger or in addition suppresser of the macrovoids present in the membrane underneath the top layer (i.e., sublayer) (Machado *et al.* 1999). In the present study, it is possible that for both PS/DMAc/PEG/D-TA and PS/DMAc/PEG/DL-TA system have a membrane with a very well permeable substructure owing to the presence of increased number of macrovoids which may be larger than the voids created by PEG alone. Between D-TA and DL-TA membranes former gave better pore structure may be because of its more solubility than DL-TA.

Fig. 8 also depicts the effect of addition of D-TA and DL-TA or chirality of TA on PWF at different trans membrane pressures (TMP). PWF (calculated using Eq. (1)) found to be increased with increase in TMP. PWF was lowest for PS/DMAc/PEG membrane; this finding is in agreement to the compaction study. For example, at 345 kPa, the PWF increases from 30.4 Lm<sup>-2</sup> h<sup>-1</sup> to 94.82 Lm<sup>-2</sup> h<sup>-1</sup> for membrane M-1 and M-2, respectively.

Hydraulic resistance ( $R_m$ ) is also an important consideration for finding the HPCT of membranes. It was calculated using Eq. (2). It was found that hydraulic resistance ( $R_m$ ) was decreasing by the addition of TA and consequently flux was increasing. Water molecules accommodated in the pores present on the membrane surface also in the porous structure of the sublayer (Sivakumar *et al.* 1999) and addition of TA increases the number of pores on the top layer as well as in the sublayer. By the addition of D-TA and DL-TA,  $R_m$  was found to be decreased; however D-TA gave better result than DL-TA.  $R_m$  for membrane M-1, M-2, M-3, M-4 and M-5 was calculated as  $4.6 \times 10^{12}$  (m<sup>-1</sup>),  $1.5 \times 10^{12}$  (m<sup>-1</sup>),  $2.1 \times 10^{12}$  (m<sup>-1</sup>),  $2.8 \times 10^{12}$  (m<sup>-1</sup>) and  $3.1 \times 10^{12}$  (m<sup>-1</sup>), respectively. Fouled resistance  $R_f$  for membrane M-1, M-2, M-3, M-4 and M-5 was

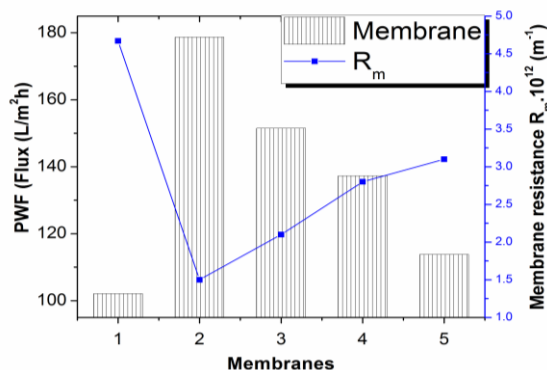


Fig. 9 PWF for all the membranes after compaction (at 345 kPa), at 208 kPa and 1h and  $R_m$

also calculated. It was calculated as  $13.5 \times 10^{12}$  (m<sup>-1</sup>),  $4.3 \times 10^{12}$  (m<sup>-1</sup>),  $6.1 \times 10^{12}$  (m<sup>-1</sup>),  $8.2 \times 10^{12}$  (m<sup>-1</sup>) and  $9.1 \times 10^{12}$  (m<sup>-1</sup>), respectively. These results clearly depict the increased HPCT of fabricated membranes by the addition of both D-TA and DL-TA.

Lower flux was found as the hydraulic resistance increased with addition of DL-TA as compared to the addition of D-TA may be due to the solubility of it in water, as it is less soluble than D-TA, it remains inside the pore with PEG and reduced the sublayer pore length. However the top layer pores were bigger and pores present in per unit square area were less on top surface as shown in FESEM images depicted in Fig. 4. Whereas, decrease in hydraulic resistance and therefore elevated flux by the addition of D-TA may due to the fact that it is highly soluble in water and since having less molecular size it creates smaller pores on the top layer it does not remain inside the pores with or without PEG and increased the sublayer pore size thus, pores present in per square area on the top surface were more as shown in FESEM images depicted in Fig. 4. In the present study, perhaps swelling of PEG molecules (knotted inside the membrane matrix) with DL-TA molecules predominantly took place as a result of its hygroscopic and hydrophilic nature. This followed by blocking of pores and subsequently in flux reduction (Chun *et al.* 2004).

### 3.3.3 Effect of chirality of TA on the flux and rejection behaviour of all the membranes

Fig. 9 shows the pure water flux after compaction (for 1 h at 345 kPa). It was observed that flux was least for PS/DMAc/PEG membrane and both the D-TA containing membranes show higher flux because of the fact that addition of two or more additives in casting solution may increase the porosity of the membranes discussed in earlier section. Membrane resistance was also found to be decreased by the addition of both the TAs. It may be because of the increased HPCT of TA containing membranes. Afterwards, BSA rejection at normal pH (i.e., at pH 7) of all the 5 membranes was also measured by collecting the permeate for 1 h. Fig. 10 depicts the flux and rejection (%) of BSA and it was observed that maximum BSA flux and rejection (%) occurred on M-2 membrane which contains D-TA 1 wt% and PEG (400 Da). BSA flux and rejection (%) trend was just opposite for the D-TA containing membrane from the mere PEG containing membrane. Rejection % was enhanced with increasing the concentration of D-TA in membrane. It may be described by the fact that thermodynamic and rheological changes may affect the morphology of the membrane as two additives (i.e., PEG and D-TA or DL-TA) were added in casting solution (Sharma *et al.* 2015).

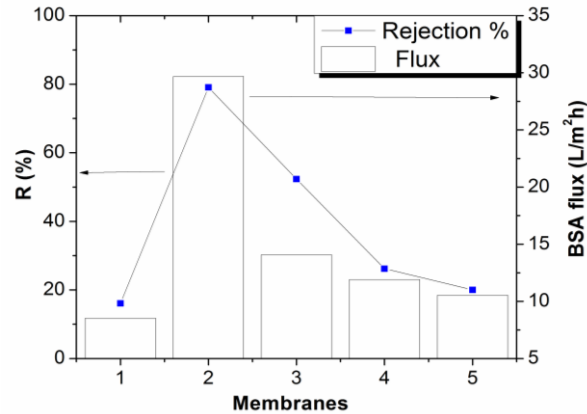


Fig. 10 BSA flux and rejection for all the membrane at 208 kPa and pH7 for 1h and 1000mg/L BSA concentration

Table 3 Values of some characterization parameters of all the 5 membranes

Membrane	EWC (%)	$R_m \times 10^{-12}$ (m <sup>-1</sup> )	CF	IEC	Contact angle (°)
M-1	18.3	4.6	4.3	0.07	79
M-2	45.9	1.5	2.7	0.65	57
M-3	42.1	2.1	2.75	0.35	61
M-4	26.8	2.8	2.9	0.29	68
M-5	22.4	3.1	3.1	0.25	71

### 3.4 Characterization of membranes on the basis of EWC, HPCT and porosity

#### 3.4.1 Effect of the addition of TAs on EWC

For finding the EWC of all the membranes standard equation (Sharma *et al.* 2015) was used and calculated values are placed in Table 3. Observations show that by the addition of D-TA EWC (%) have increased from 18.3 to 45.9 and 42.1 for membrane M-1, M-2 and M-3, respectively. This tendency confirms the increasing number of pores in the membrane with addition of D-TA (Table 2). The pores formed on the surface as well as macrovoids in the sublayer during wet phase inversion process are helpful for compliant water molecules in the membrane (Sivakumar *et al.* 1999). Addition of DL-TA into the membrane matrix also increased the EWC from 18.3 to 26.8, 22.4 for membrane M-1, M-4 and M-5, respectively. However, D-TA containing membranes have shown better EWC than membranes with DL-TA. This may be attributed to the reality that D-TA molecules may have circulate into the PEG molecule and in membrane matrix and during immersion of casted membrane in water (phase inversion) they got released from the membrane and mostly from the top surface and disturb the network on the other hand DL-TA molecules could not disperse in the same amount into the coagulation bath since, their solubility in water is less than D-TA. Hydrogen bonds between PEG and TA may first formed during preparation of membrane casting solution and have been broken during immersion of membrane into the coagulation bath and some TA molecules came out to the surface of membrane, hence 1 wt% D-TA with PEG (400 Da) containing membrane formed more pores which are smaller in size, on the surface of membrane.

### 3.4.2 Effect of addition of TAs on HPCT

Role of HPCT and porosity of the membrane is undoubtedly significant in membrane permeation performance. Contact angle measurement is a potential tool for finding the surface HPCT (Zheng *et al.* 2006). Generally it is a common phenomenon that the HPCT increases as the value of contact angle decreases. Contact angle of membranes without any kind of TA and with different concentration of D-TA and DL-TA are shown in Table 3. It can be resulted from Table that contact angle decreased with the addition of both D-TA and DL-TA. However, D-TA containing membranes showed more reduced contact angles and increased porosity than membranes having DL-TA. The contact angle for M-1, M-2, M-3, M-4 and M-5 was 79°, 57°, 61°, 68° and 71°, respectively.

### 3.4.3 Effect of TAs on porosity

Porosity was found to be increased by the addition of both the TAs (Table 2). Increase in porosity may be due the fact that they disturbed the thermodynamic equilibrium of membrane casting solution with coagulation bath during membrane formation by wet phase inversion method, as discussed in the previous section. The porosity changes can also explain with the help of kinetic consideration. Presence of additives into the casting solution can cause two alterations. Firstly, the reduced miscibility of the casting solution in nonsolvent due to phase separation since the thermodynamic improvement occurs. Secondly, it produces kinetic obstruction to phase separation because of the increased viscosity of the solution (Mulder 1996). Viscosity of casting solution prepared by blending of different ingredients was measured as 0.879 Pa s, 0.921 Pa s, 0.911 Pa s, 0.928 Pa s and 0.919 Pa s for M-1, M-2, M-3, M-4 and M-5, respectively. It confirmed from SEM images shown in Fig. 3 that by the addition of D-TA top layer got reduced and sublayer pores became more regular.

## 3.5 Ultrafiltration of BSA

TMP is a key factor for finding the characteristic of flux other than that, quality of flux and solute retention through the membranes mainly assessed by the feed solution characteristics, specially its pH. Concentration of BSA solution was taken as 1000 mg/L.

### 3.5.1 Effect of D-TA and DL-TA concentration on BSA rejection

Fig. 11 shows the effect of two different concentrations of D-TA and DL-TA on the rejection profile of BSA at normal pH (i.e., pH 7). It was observed that the rejection was constant after 4h for all membranes. Maximum rejection was achieved by membrane M-2; i.e., by increasing the concentration of D-TA and DL-TA the rejection was found to be increased, it may be attributed to the fact that hydrophilic functional groups of both TAs were increased into the PS casting solution. However, addition of DL-TA showed the lower rejection than D-TA containing membranes because of the formation of larger pores on the top surface of membranes. For example rejection (%) for M-1, M-2, M-3, M-4 and M-5 was found as 22.5%, 78.1%, 75.4%, 51.7% and 36%, respectively. By reducing the TA concentration the rejection (%) was also declined. For instance % *R* for M-3 and M-5 was measured as 75.4% and 36%, respectively. It may be because of the fact that presence of hydrophilic group was lowered on the membrane surface by decreasing the TA concentration in casting solution. Moreover, addition of organic acid altered the membrane morphology as well as skin-layer thickness (Fig. 3) and hence higher porosity was formed (Table

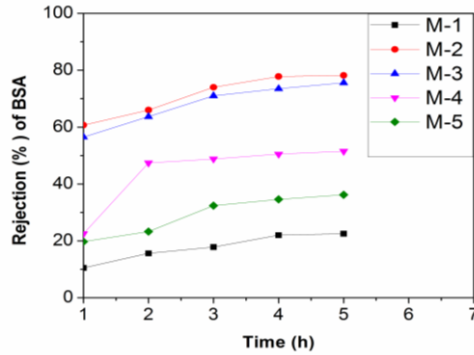


Fig. 11 BSA Rejection profile at normal pH

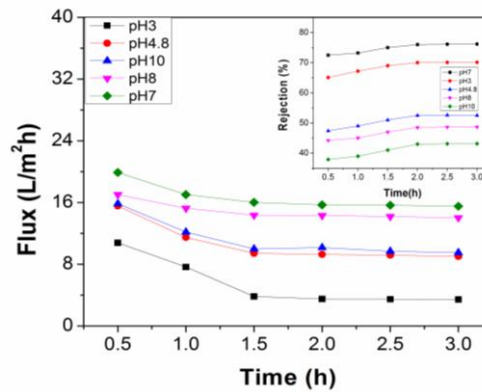


Fig. 12 Effect of pH on BSA flux and rejection for M-2 membrane

2). Varying morphology possesses a significant control over increment of PWF of the modified membranes. However, rejection (%) is low for membrane M-1, it may be due to the fact that some bigger pores are present on the membrane surface (Fig. 4). These pores might be responsible for lower rejection. Mean pore size was measured 12.43 nm, for membrane M-1 by FESEM image analysis.

Values of zeta potential (ZP) also play important role in rejection performance of the membrane. ZP was found to be increased by the addition of both D-TA and DL-TA in membrane casting solution. At pH 7.5 it was measured as -8.11 mV, -18.39 mV, -17.16 mV, -17.58 mV and -16.75 mV for M-1, M-2, M-3, M-4 and M-5, respectively. So due to elevated ZP negative charge ( $\text{OH}^-$ ) also increases for acid containing membrane. Since, carbonyl groups present in carboxylic acid electrophilic in nature which results in increased  $\text{OH}^-$  in carboxylic acid (Ghaemi *et al.* 2012a). Therefore addition of D-TA and DL-TA in PS membranes consequences in more rejection of BSA molecules.

### 3.5.2 Effect of pH on BSA flux and rejection

Fig. 12 depicts the flux and rejection through membrane M-2 at different pH. It was observed that flux was maximum at pH 3 and minimum at pH 10, it may be approved by the fact that at basic condition (pH 10) there was a high charge density at the surface of the membrane because, at

pH 10 there was increased negative charge in solution and negative charge already present on membrane surface (Table 2). Elevated ion density on the top layer of the membrane obstructs the permeation, consequently reduced flux was observed. Whereas, at pH 3 there was a lowest charge density on the membrane surface hence highest flux was achieved. At pH 8 and 7 flux was moderate due to electrostatic charge repulsion (since BSA molecules have elevated net negative charge) (Fane *et al.* 1981, Musale *et al.* 1997, Ghosh *et al.* 1998). At iso-electric point (IEP) BSA molecules are least soluble and they do not have any charge in this condition. They accumulated in a compact layer which is mostly responsible for lower flux and higher BSA rejection at 4.8 than at pH 3.

Charge density in the membranes can be found by IEC. It also affects their fouling behavior. IEC was measured by standard technique (Yan *et al.* 2012). Table 3 illustrates the IEC of different membranes; IEC for membranes M-1, M-2, M-3, M-4 and M-5 were 0.07, 0.65, 0.35, 0.29 and 0.25, respectively. It clearly shows that IEC increasing with increasing the concentration of D-TA (1 wt %) in the membranes. This fact can be explained with the help of ionization behavior of D-TA present in membrane matrix of M-2, M-3, M-4 and M-5. Variation in BSA solution flux at different pH may be described by protonation and deprotonation potential of D-TA. Deprotonation of carboxylic groups of TA resulted in carboxylate ions. These carboxylate ions offer excessive charge in the PEG/D-TA containing membranes.

Right part of Fig. 12 depicts the rejection behavior of BSA solution at different pH for membrane M-2. Rejection of BSA molecules with the pH was found in the sequence of  $10 > 8.0 > 7 > 4.8 > 3$ . Rejection was found to be lowest at lowest pH (i.e., pH 3) it may be because of the fact that pores become bigger at extreme acidic condition due to collapse of PEG/D-TA molecules and thus fallout in lower rejection of BSA (Hunter 1981). At IEP (i.e., pH 4.8) BSA is least soluble and hence accumulated on the surface of membrane and results in lowering flux and moderate rejection than pH 3 and pH 10. The highest rejection of BSA molecules in extreme basic solution condition (pH 10) might be explained by the fact that at this pH feed solution had net negative ions and deprotonation of D-TA was occurred and robust electrostatic charge revulsion between negative charges of the membrane surface and negative BSA molecules (Ghaemi *et al.* 2012a).

### 3.6 Reversible and irreversible fouling study

For finding the fouling values, pH of 7 was used during experiments. The time dependent flux of membranes modified by the blending of D-TA and DL-TA is shown in Fig. 13 Deionized water flux ( $J_{w1}$ ) was measured from 0-60 min, 180-240 min ( $J_{w2}$ ), and BSA flux was measured from 60-180 min and 240-360 min. Water permeation results were showing a slight loss of flux through initial time of water permeation and after that it remains constant for all the membranes, but during BSA permeation, a severe flux loss was seen in initial permeation for all the membranes. Initial loss of flux during UF of BSA may be because of the deposition or adsorption of BSA molecules on the surface of membranes or inside the pores. So, the fouling resistance membrane should successfully oppose the deposition or adsorption of foulants to their surface or pore as reported in literatures (Li *et al.* 2013, Huisman *et al.* 2000).

For investigating the fouling resistant behaviour of the membrane,  $F_r$  and  $F_{ir}$  values were calculated from Fig. 13 using Eqs. (13), (14) and are shown in Fig. 14. It can be seen in Fig. 14 that by the addition of D-TA and DL-TA in modified membranes,  $F_{ir}$  values are reduced significantly as compared to plain membrane and therefore, the  $F_r$  values are increased. Furthermore the sequence of fouling values is consistent with hydrophilicity and BSA rejection

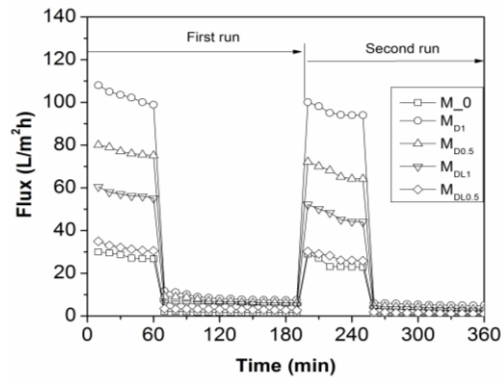


Fig. 13 Time dependent flux of membrane during ultrafiltration

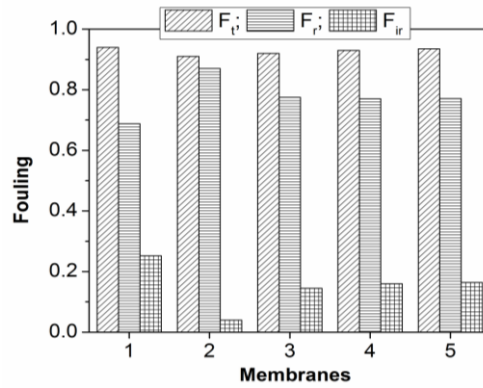


Fig. 14 Effect of TAs on fouling parameters

trend of membranes. In this case, the hydrophilic segment of the TAs could form hydration layer on the membrane surface through hydrogen bonding, exhibiting anti fouling property and efficiently prevent adsorption deposition of foulants. Sharma *et al.* (2017) also observed the similar result by the blending of amphiphilic amino alcohol plasticizer with PSF membrane. However, it can be remarked that  $F_r$  values increased after addition of both the TAs. The possible reason could be accumulation of more BSA on membrane surface due to comparatively increased BSA rejection. Even though increased  $F_r$  value, the value of total fouling showed a reducing trend due to remarkable decrease in  $F_{ir}$  value. So, these trends suggest that anti fouling property, especially irreversible fouling of modified PSF membrane was enhanced appreciably by the blending of TAs.

#### 4. Conclusions

Effects of D-TA and DL-TA (i.e., effect of chirality) on the morphology such as pore number, pore area and porosity in terms of average pore size of PS membrane were checked in detail. Effect of wt % of both the TAs in membrane morphology were measured and following observations were made:

- (i) Both D-TA and DL-TA were responsible for pore size reduction on the membrane surface. But, FESEM images confirm the fact that it was minimum by the addition of D-TA. Thus, chirality influenced the morphology of membrane.
- (ii) The PWF, hydraulic permeability, EWC (%) increased and hydraulic resistance  $R_m$  decreased with increasing the wt % of D-TA as well as DL-TA from 0.5 to 1 wt % and subsequently depicted increase in HPCT and porosity of the membranes.
- (iii) Maximum porosity was observed for PEG (400 Da) with D-TA (1 wt %). Porosity was found to be increased by the addition of both D-TA and DL-TA. However, it was found lower by the addition of DL-TA as compared to D-TA addition.
- (iv) At normal solution pH (i.e., pH 7) BSA rejection was found maximum for M-2 membrane. Further study the effect of pH on the selected M-2 membrane revealed the fact that BSA flux was maximum at acidic pH (i.e., pH 3). Order of BSA flux was  $3 > 4.8 > 7 > 8 > 10$  and BSA rejection was highest at basic pH conditions, the order of pH with respect to the BSA rejection was as  $10 > 8 > 7 > 4.8 > 3$ .

## Acknowledgements

This work is partially supported by a grant from the Indian National Science Academy (INSA), New Delhi. Any opinions, findings and conclusions expressed in this article are those of the authors and do not necessarily reflect the views of INSA, New Delhi.

## References

- Abaticchio, P., Bottino, A., Capannelli, G. and Munari, S. (1990), "Characterization of ultrafiltration polymeric membranes", *Desalinat.*, **78**, 235-255.
- Ahmad, A.L., Abdulkarim, A.A., Ooi, B.S. and Ismail, S. (2013), "Recent development in additives modifications of polyethersulfone membrane for flux enhancement", *Chem. Eng. J.*, **223**, 246.
- Bhadra, S., Singha, N.K. and Khastgir, D. (2008), "Effect of aromatic substitution in aniline on the properties of polyaniline", *Eur. Poly. J.*, **44**, 1763.
- Calvo, J., Bottino, A., Capannelli, G. and Hernández, A. (2004), "Comparison of liquid-liquid displacement porosimetry and scanning electron microscopy image analysis to characterise ultrafiltration track-etched membranes", *J. Membr. Sci.*, **239**(2), 189-197.
- Capannelli, G., Vigo, F. and Munari, S. (1983), "Ultrafiltration membranes- characterization methods", *J. Membr. Sci.*, **15**, 289-313.
- Chakrabarty, B., Ghoshal, A.K. and Purkait, M.K. (2008), "Preparation, characterization and performance studies of polysulfone membranes using PVP as an additive", *J. Membr. Sci.*, **315**, 36-47.
- Cheryan, M. (1998), *Ultrafiltration and Microfiltration Handbook*, Technomic Publishing Company Inc. USA, 345.
- Chun, M.K., Cho, C.S. and Choi, H.K. (2004), "Characteristics of poly (vinyl pyrrolidone)/poly(acrylic acid) interpolymer complex prepared by template polymerization of acrylic acid: Effect of reaction solvent and molecular weight of template", *J. Appl. Poly. Sci.*, **94**, 2390-2394.
- Duarte, A.R.C., Mano, J.F. and Reis, R.L. (2012), "The role of organic solvent on the preparation of chitosan scaffolds by supercritical assisted phase inversion", *J. Superc. Fluid.*, **72**, 326-332.
- Fane, A.G., Fell, C.J.D. and Waters, A.G. (1981), "The relationship between membrane surface pore characteristics and flux for ultrafiltration membranes", *J. Membr. Sci.*, **9**, 245-262.
- Geise, G.M., Lee, H.S., Miller, D.J., Freeman, B.D., McGrath, J.E. and Paul, D.R. (2010), "Water

- purification by membranes: the role of polymer science”, *J. Poly. Sci. Part B: Polym. Phys.*, **48**, 1685.
- Ghaemi, N., Madaeni, S.S., Abdolhamid, A., Rajabi, H., Daraei, P. and Falsafi, M. (2012), “Effect of fatty acids on the structure and performance of cellulose acetate nano filtration membranes in retention of nitroaromatic pesticides”, *Desalinat.*, **301**, 26-41.
- Ghaemi, N., Madaeni, S.S., Alizadeh, A., Daraei, P., Badieh, M.M.S., Falsafi, M. and Vatanpour, V. (2012), “Fabrication and modification of polysulfone nanofiltration membrane using organic acids: Morphology, characterization and performance in removal of xenobiotics”, *Separat. Purif. Technol.*, **96**, 214-228.
- Ghosh, R. and Cui, Z.F. (1998), “Fractionation of BSA and lysozyme using ultrafiltration: effect of pH and membrane pretreatment”, *J. Membr. Sci.*, **139**, 17-28.
- Hand, A.J., Sun, T., Barber, D.C., Hose, D.R. and MacNeil, S. (2009), “Automated tracking of migrating cells in phase-contrast video microscopy sequences using image registration”, *J. Micros.*, **234**, 62-79.
- Huisman, J.H., Pradanos, P. and Hermandez, A. (2000), “The effect of protein-protein and protein-membrane interactions on membrane fouling in ultrafiltration”, *J. Membr. Sci.*, **179**, 79-90.
- Hunter, R.J. (1981), *Zeta Potential in Colloid Science*, Academic Press, London.
- Ingole, P.G., Sawant, S.Y., Ingole, N.P., Pawar, R.R., Bajaj, H.C., Singh, K., ... & Lee, H.K. (2016), “Preparation of activated carbon incorporated polysulfone membranes for dye separation”, *Membr. Water Treat.*, **7**(6), 477-493.
- Kamusewitz, H., Schossig-Tiedemann, M., Keller, M. and Paul, D. (1997), “Characterization of polymeric membranes by means of scanning force microscopy (SFM) in comparison to results of scanning electron microscopy (SEM)”, *Surf. Sci.*, **377-379**, 1076-1081.
- Kim, J.H. and Lee, K.H. (1998), “Effect of PEG additive on membrane formation by phase inversion”, *J. Membr. Sci.*, **138**, 153-163.
- Kimmerle, K. and Strathmann, H. (1990), “Analysis of the structure-determining process of phase inversion membranes”, *Desalinat.*, **79**, 283-302.
- Kobayashi, T., Reddy, P.S., Ohta, M., Abe, M. and Fujii, N. (2002), “Molecularly imprinted polysulfone membranes having acceptor sites for donor dibenzo furan as novel membrane adsorbents: charge transfer interaction as recognition origin”, *Chem. Mater.*, **14**, 2499-2505.
- Li, Q., Bi, Q., Lin, H., Bian, L. and Wang, X. (2013), “A novel ultrafiltration (UF) membrane with controllable selectivity for protein separation”, *J. Membr. Sci.*, **427**, 155-167.
- Li, Y.S., Yan, L., Xiang, C.B. and Hong, L.J. (2006), “Treatment of oily wastewater by organic-inorganic composite tubular ultrafiltration (UF) membranes”, *Desalinat.*, **196**, 76-83.
- Li1, J., Nie, S., Wang, L., Sun, S., Ran, F. and Zhao, C. (2013), “One-pot synthesized poly(vinyl pyrrolidone-co-methyl methacrylate-co-acrylic acid) blended with poly(ether sulfone) to prepare blood-compatible membrane”, *J. Appl. Poly. Sci.*, **130**, 39463-39472.
- Liou, R.M., Chen, S.H., Lai, C.L., Hung, M.Y. and Huang, C.H. (2011), “Effect of ammonium groups of sulfonated polysulfone membrane on its pervaporation performance”, *Desalinat.*, **278**, 91-97.
- Machado, P.S.T., Habert, A.C. and Borges, C.P. (1999), “Membrane formation mechanism based on precipitation kinetics and membrane morphology: flat and hollow fiber polysulfone membranes”, *J. Membr. Sci.*, **155**, 171-183.
- Mansourizadeh, A. and Ismail, A.F. (2010), “Effect of additives on the structure and performance of polysulfone hollow fiber membranes for CO<sub>2</sub> absorption”, *J. Membr. Sci.*, **348**, 260-267.
- Mulder, M. (1996), *Basic Principles of Membrane Technology*, Kluwer Academic Publishers, Netherlands **56**, 49-51.
- Musale, D.A. and Kulkarni, S.S. (1997), “Relative rates of protein transmission through poly (acrylonitrile) based ultrafiltration membranes”, *J. Membr. Sci.*, **136**, 13-23.
- Qiu, S., Wu, L.G., Pan, X.J., Zhang, L., Chen, H.L. and Gao, C.J. (2009), “Preparation and properties of functionalized carbon nanotube/PSF blend ultrafiltration membranes”, *J. Membr. Sci.*, **342**, 165-172.
- Reuvers, J. and Smolders, C.A. (1987), “Formation of membranes by means of immersion precipitation. Part II. The mechanism of formation of membranes prepared from the system cellulose acetate- acetone-water”, *J. Membr. Sci.*, **34**, 67-86.
- Sevilla, P., Rivas, J.M., García-Blanco, F., García-Ramos, J.V. and Sánchez-Cortés, S. (2007),

- “Identification of the antitumoral drug emodin binding sites in bovine serum albumin by spectroscopic methods”, *Biochem. Biophys. Acta*, **1774**, 1359-1369.
- Sharma, N. and Purkait, M.K. (2015), “Preparation of hydrophilic polysulfone membrane using polyacrylic acid with polyvinyl pyrrolidone”, *J. Appl. Poly. Sci.*, **132**, 41964-41976.
- Sharma, N. and Purkait, M.K. (2016), “Enantiomeric and racemic effect of tartaric acid on polysulfone membrane during crystal violet dye removal by MEUF process”, *J. Water Proc. Eng.*, **10**, 104-112.
- Sharma, N. and Purkait, M.K. (2016), “Racemic and enantiomeric effect of tartaric acid on the hydrophilicity of polysulfone membrane”, *Membr. Water Treat.*, **7**(3), 257-275.
- Sharma, N. and Purkait, M.K. (2017), “Impact of synthesized amino alcohol plasticizer on the morphology and hydrophilicity of polysulfone ultrafiltration membrane”, *J. Membr. Sci.*, **522**, 202-215.
- Silverstein, R.M., Bassler, G.C. and Morrill, T.C. (1991), *Spectrometric Identification of Organic Compounds*, John Wiley & Sons Inc., New York.
- Sinha, M.K. and Purkait, M.K. (2015), “Preparation of fouling resistant PSF flat sheet UF membrane using amphiphilic polyurethane macromolecules”, *Desalinat.*, **355**, 155-168.
- Sinha, M.K. and Purkait, M.K. (2013), “Increase in hydrophilicity of polysulfone membrane using polyethylene glycol methyl ether”, *J. Membr. Sci.*, **437**, 7-16.
- Sivakumar, M., Malaisamy, R., Sajitha, C.J., Mohan, D., Mohan, V. and Rangarajan, R. (1999), “Ultrafiltration application of cellulose acetate-polyurethane blend membranes”, *Euro. Polym. J.*, **35**, 1647-1651.
- Stuart, B. (2004), *Infrared Spectroscopy: Fundamentals and Applications*, John Wiley & Sons, Ltd.
- Tweddle, T.A., Kutowy, O., Thayer, W.L. and Sourirajan, S. (1983), “Polysulfone ultrafiltration membranes”, *Ind. Eng. Chem. Product Res. Dev.*, **22**, 320-326.
- Vatanpour, V., Madaeni, S.S., Moradian, R., Zinadini, S. and Astinchap, B. (2012), “Novel antifouling nanofiltration polyether sulfone membrane fabricated from embedding TiO<sub>2</sub> coated multiwalled carbon nanotubes”, *Separat. Purif. Technol.*, **90**, 69-82.
- Wang, J.Y., Xu, Y.Y., Zhu, L.P., Li, J.H. and Zhu, B.K. (2008), “Amphiphilic ABA copolymers used for surface modification of polysulfone membranes, Part 1: Molecular design, synthesis, and characterization”, *Polym.*, **49**, 3256-3264.
- Wang, Y., Wang, T., Su, Y., Peng, F., Wu, H. and Jiang, Z. (2005), “Remarkable reduction of irreversible fouling and improvement of the permeation properties of poly(ether sulfone) ultrafiltration membranes by blending with pluronic F127”, *Langmuir*, **21**, 11856-11862.
- Wei, X., Wang, Z., Wang, J. and Wang, S. (2012), “A novel method of surface modification to polysulfone ultrafiltration membrane by preadsorption of citric acid or sodium bisulfite”, *Membr. Water Treat.*, **3**, 35-49.
- Yan, X., He, G., Gu, S., Wua, X., Dua, L. and Wang, Y. (2012), “Imidazolium-functionalized polysulfone hydroxide exchange membranes for potential applications in alkaline membrane direct alcohol fuel cells”, *Int. J. Hydro. Energy*, **37**, 5216-5224.
- Yang, L., Chen, X.Q. and Jiao, F.P. (2009), “Extractive resolution of racemic mandelic acid through a bulk liquid membrane containing binary chiral carrier”, *J. Braz. Chem. Soc.*, **8**, 1493-1498.
- Zhang, Y., Shana, L., Tua, Z. and Zhang, Y. (2008), “Preparation and characterization of novel Ce doped non stoichiometric nano silica/polysulfone composite membranes”, *Separat. Purif. Technol.*, **63**, 207-212.
- Zheng, Q.Z., Wang, P. and Yang, Y.N. (2006), “Rheological and thermodynamic variation in polysulfone solution by PEG introduction and its effect on kinetics of membrane formation via phase-inversion process”, *J. Membr. Sci.*, **279**, 230-237.